International Journal of Bioprinting

REVIEW ARTICLE

State-of-the-art techniques for promoting tissue regeneration: Combination of three-dimensional bioprinting and carbon nanomaterials

Iruthayapandi Selestin Raja[1†], Moon Sung Kang[2†], Suck Won Hong[2], Hojae Bae[3], Bongju Kim[4], Yu-Shik Hwang[5], Jae Min Cha[6*], Dong-Wook Han[1,2*]

[1]BIO-IT Fusion Technology Research Institute, Pusan National University, Busan 46241, South Korea

[2]Department of Cogno-Mechatronics Engineering, College of Nanoscience & Nanotechnology, Pusan National University, Busan 46241, South Korea

[3]Department of Stem Cell and Regenerative Biotechnology, KU Convergence Science and Technology Institute, Konkuk University, Seoul, 05029, Republic of Korea

[4]Dental Life Science Research Institute/Innovation Research & Support Center for Dental Science, Seoul National University Dental Hospital, Seoul 03080, South Korea

[5]Department of Maxillofacial Biomedical Engineering and Institute of Oral Biology, School of Dentistry, Kyung Hee University, Seoul 02447, South Korea

[6]Department of Mechatronics Engineering, College of Engineering, Incheon National University, Incheon 22012, South Korea

(This article belongs to the *Special Issue: Functional Bioprinting Systems for Tissue Engineering*)

[†]These authors contributed equally to this work.

***Corresponding authors:**
Jae Min Cha (j.cha@inu.ac.kr)
Dong-Wook Han (nanohan@pusan.ac.kr)

Citation: Raja IS, Kang MS, Hong SW, *et al*., 2023, State-of-the-art techniques for promoting tissue regeneration: Combination of three-dimensional bioprinting and carbon nanomaterials. *Int J Bioprint*, 9(1): 635.
https://doi.org/10.18063/ijb.v9i1.635

Received: July 04, 2022
Accepted: August 23, 2022
Published Online: November 4, 2022

Abstract

Biofabrication approaches, such as three-dimensional (3D) bioprinting of hydrogels, have recently garnered increasing attention, especially in the construction of 3D structures that mimic the complexity of tissues and organs with the capacity for cytocompatibility and post-printing cellular development. However, some printed gels show poor stability and maintain less shape fidelity if parameters such as polymer nature, viscosity, shear-thinning behavior, and crosslinking are affected. Therefore, researchers have incorporated various nanomaterials as bioactive fillers into polymeric hydrogels to address these limitations. Carbon-family nanomaterials (CFNs), hydroxyapatites, nanosilicates, and strontium carbonates have been incorporated into printed gels for application in various biomedical fields. In this review, following the compilation of research publications on CFNs-containing printable gels in various tissue engineering applications, we discuss the types of bioprinters, the prerequisites of bioink and biomaterial ink, as well as the progress and challenges of CFNs-containing printable gels in this field.

Keywords: Carbon-family nanomaterial; Bioprinting; Tissue engineering; Bioink; Biomaterial ink

1. Introduction

Three-dimensional (3D) bioprinting, as a subset of additive manufacturing, has become an emerging technology in many biomedical applications, including tissue engineering

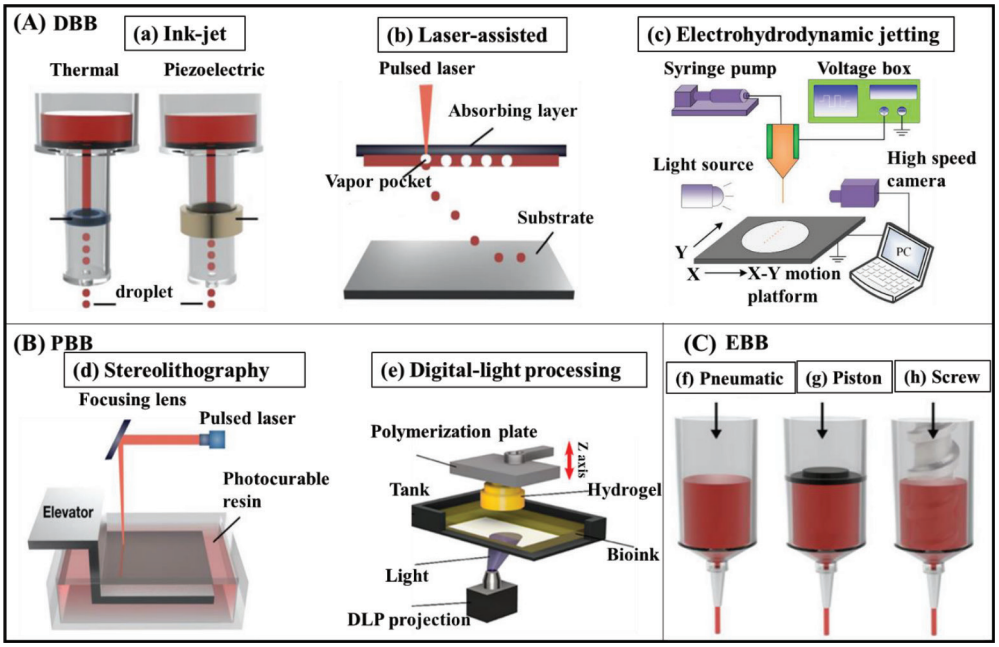

Figure 1. Schematic illustration of 3D bioprinting systems. (A) Droplet-assisted bioprinting (DBB) includes (a) ink-jet, (b) laser-assisted, and (c) electrohydrodynamic jetting. (B) Photocuring-based bioprinting (PBB) includes (d) stereolithography and (e) digital-light processing. (C) There are three types of extrusion-based bioprinting (EBB), which are (f) pneumatic, (g) piston, and (h) screw. Images (a), (b), (d), (f), (g), and (h) were reprinted from *Bioengineering*, 7, Jeong HJ, Nam H, Jang J, *et al*., 3D Bioprinting strategies for the regeneration of functional tubular tissues and organs, 32, Copyright (2020), with permission from MDPI[23]. Image (c) was reprinted from *Micromachines*, 10, Pan Y, Zeng L, Simulation and validation of droplet generation process for revealing three design constraints in electrohydrodynamic jet printing, 94, Copyright (2019), with permission from MDPI[20]. Image (e) was reprinted from *International Journal of Molecular Sciences*, 23, Seo JW, Kim GM, Choi Y, *et al*., Improving printability of digital-light-processing 3D bioprinting via photoabsorber pigment adjustment, 5428, Copyright (2022), with permission from MDPI[29].

(TE) and regenerative medicine. Unlike conventional additive manufacturing techniques, tailored and precise constructs can be fabricated by simply controlling the printing parameters, such as biocompatible materials, instrumental methods (temperature, pressure, and speed), and employed cells[1-3]. 3D bioprinting primarily involves layer-by-layer deposition of cell-free or cell-laden biocompatible materials in predetermined computer-designed structural constructs to fabricate functional tissue analogs[4-6]. Moreover, 3D bioprinting in TE has some advantages in developing complex biological structures, such as high fidelity, low material loss, patient-specific designs, and tailored fabrication within a short period of time[7].

1.1. Types of bioprinting

3D bioprinting techniques can be classified into three types according to different molding principles: droplet-based bioprinting (DBB), photocuring-based bioprinting (PBB), and extrusion-based bioprinting (EBB)[8,9], as shown in Figure 1.

1.1.1. Droplet-based bioprinting

Inkjet, laser-assisted, and electrohydrodynamic jetting bioprinters are used in DBB technologies[10]. Inkjet bioprinting can be divided into drop-on-demand (DOD) and continuous inkjet (CIJ) printings. In DOD printing, the bioprinter produces bioink droplets over the substrate whenever required, whereas in CIJ printing, ink droplets are continuously dispersed from a liquid stream flow. DOD printing is efficient for several-layered deposition of material and fine patterning, owing to its high precision and minimal waste of bioink. Thermal, electrostatic, or piezoelectric forces are used in this technique to produce and deposit droplets of various biological materials to construct a spatially heterogeneous tissue structure[11,12]. Recently, Binder *et al*. demonstrated that the deposition of printable bioink containing human keratinocytes and fibroblasts over full-thickness skin defects of athymic mice using DOD technology stimulated wound healing and reduced skin contracture[13]. However, DOD has some limitations, including small inkjet apertures (10–150 μm) and the production of nonporous tissue-engineered structures, which may affect tissue perfusion and substance exchange. Hence, only low-viscosity hydrogels can be used for DOD printing. In addition, the drop rate of DOD printing is lower than that of CIJ printing[14].

In laser-assisted bioprinting, the system contains a pulsed laser source, a focusing tool, a metallic ribbon film

on the back of the silicate glass, and a substrate receiver. The focused laser beam on the metal film induces local heating and subsequently evaporates the bioink deposited on the glass, which is then sprayed onto the substrate as liquid drops[15,16]. Koch *et al.* employed laser-assisted printing to print skin fibroblast cells and human mesenchymal stem cells (hMSCs) and reported a cell survival rate of ~98% and ~90%, respectively[17]. The main advantage of the system is that picogram-level printing resolution can be achieved using a nanosecond laser with an ultraviolet (UV) energy wavelength. Furthermore, the equipment does not have a nozzle, and thus performs noncontact printing. The disadvantage of laser-assisted bioprinting is the slow gelation mechanism, which limits its high-throughput printing[18,19].

In electrohydrodynamic jetting (EHDJ), the metallic nozzle is loaded with bioink to form a spherical meniscus at the nozzle tip. An electric field is created on the meniscus by generating a high voltage between the nozzle and substrate. The accumulated mobile ions at the meniscus deform into the Taylor cone due to electrostatic repulsions, and the droplets are ejected under an optimized voltage[20]. The bioink adopts different modalities, such as Taylor jetting, intermittent jetting, micro-dripping, unsteady status, and breakdown, depending on the voltage[21]. In EHDJ bioprinting, the size of droplets and the concentration of cells affect the viability of cells. In addition, material propagation significantly reduces when the droplet size is above 400 μm[22]. The advantage of EHDJ is that the process prevents excessive pressure, which may be destructive to the cells. This method is selected for printing bioink through a small orifice with large cell concentration and a high weight-to-volume ratio[20].

1.1.2. Photocuring-based bioprinting

PBB is an approach of bioprinting that engages the photopolymerization property of photosensitive polymers under precisely controlled light without the issues of nozzle plugging and shear stress to the cells. This approach can be divided into stereolithography (SLA) and digital light processing (DLP), depending on different light scanning modes.

Charles W. Hull invented the SLA printing technology in 1984. An SLA bioprinter contains a tank filled with bioink and a platform that moves up and down while printing. The platform moves to the bioink surface and solidifies the liquid upon exposure to UV light. The precision of SLA is determined by various factors, including the scanning speed, laser power, wavelength, and exposure time[23,24]. Through this method, porous structured tissue scaffolds can be printed in high resolution of approximately 1 μm in the desired geometric shape. Rapid bioprinting and higher cell viability (>85%) without any shear force on the cells are made possible through SLA bioprinting[25,26]. The only limitation of SLA is that transparent liquid must be used to allow light to pass through the material and achieve uniform crosslinking. Hence, the maximum cell density in the bioink is restricted to approximately 10^8 cells/mL[27,28].

Unlike SLA, a DLP bioprinter immediately solidifies a complete layer, instead of point-by-point photocuring. A typical bottom-to-top DLP bioprinter prints the bottom layer first and successively each new layer over the previous one. The printing process uses a dynamic mask carrying a design pattern to transmit the light pattern to the substrate and a layering software to slice the 3D digital model to a certain thickness. Liquid crystal display, digital micromirror device, and spatial light modulator have been employed as dynamic masks in DLP printing[29]. DLP offers a remarkable advantage over DBB and EBB technologies in terms of printing speed, wherein there is no increase in printing time despite a more complex structure. Besides, DLP can fabricate a smoother 3D structure with improved structural integrity and mechanical strength, unlike the artificial interface formed between the droplets or fibers in DBB or EBB, respectively[20].

1.1.3. Extrusion-based bioprinting

In EBB, bioink containing cells is printed into a 3D construct through layer-by-layer formation with the aid of fluid distribution and automated machine systems. Under the control of a computer, bioink is passed through a micro-nozzle using piston, screw, or pneumatic approaches as a continuous filament[30,31]. Screw-driven printers produce a more stable 3D-printed tissue structure from high-viscosity bioink, whereas pneumatic-type printers inject hydrogels with shear-thinning behavior, maintaining the filament state of hydrogels even after extrusion[32]. Recently, EBB bioprinters have been designed to simultaneously deposit different bioinks with less cross-contamination using multiple printer heads[33,34]. The main advantage of EBB is the use of various types of printable bioinks, consisting of cell clumps, microcarriers, acellular matrix components, and high-viscosity hydrogels. The printing speed and mechanical strength of the structure printed by EBB are better compared to those printed by DBB[35]. Although EBB is a versatile method for fabricating prosthetic implants for TE, it has a low resolution exceeding 100 μm[36].

1.2. Printed gel properties

Among the different biomaterial forms, hydrogels are often used as printable bioinks in 3D printing because they can hold live cells, yield good resolution, and are chemically modifiable and mechanically adjustable with biodegradation properties[37,38]. Thus far, many polymeric biomaterials (natural and synthetic) have been used as a

single component or heterogeneous components combined with additives, such as copolymers, nanoparticles, and crosslinking agents[39,40]. There is less toxicity in hydrogel composites with the use of naturally available polymers, including gelatin, chitosan, alginate, and pectin. Synthetic polymers including pluronic, methacrylic acid, poly(vinyl alcohol) (PVA), and poly(ethylene glycol) (PEG) have been blended with natural polymers to increase the stability, biodegradation time, and mechanical strength of the produced hydrogel composites[41]. Gelatin methacrylate (GelMA) is a commonly employed polymeric component of printable gels in microextrusion and laser-based bioprinters because it exhibits photocurable properties by UV radiation[42,43]. Pluronic F127 (poloxamer 407) hydrogel is thermoresponsive, and it is often used as a sacrificial material, mold, and track patterning in TE[44]. When functionalized with the cell-adhesive peptide arginyl-glycyl-aspartic acid (RGD), photoactive PVA hydrogels augment cell attachment and enhance fibroblast spreading[45]. The choice of polymer affects the crosslinking reactions and mechanisms involved in printable gel. Photopolymerization is a prominent crosslink reaction in printable bioinks, as it enables control in space and during gelation[39]. Free radical polymerization of acrylate derivatives is often used to fabricate photoresponsive bioinks; however, many researchers have employed photoinitiated thiol-ene crosslinking as an alternative to the former method to form homogeneous hydrogel networks[46,47]. Thermosensitive polymers, which form supramolecular hydrogels through hydrophobic interactions within a certain temperature range, have been used in bioprinting formulations[48,49]. Small molecule-mediated cross-linkages, such as calcium chloride, glycerylphytate, and curcumin, have also supported the fabrication of printable gels with highly fine printability and customizable mechanical properties[50-52]. In order to improve viscosity and printability as well as enhance cellular activities, researchers are now creating complex 3D printable structures that incorporate nanomaterials into bioinks, which leads to the fabrication of functional tissues. Carbonaceous nanomaterials, hydroxyapatite, silica-based bioceramics, nanosilicates, bioactive glasses, strontium carbonate, and their doped nanocomposites[53-56] have been used as additives in printable inks for the fabrication of varying scaffolds for TE. In view of their biocompatibility, electrical conductivity, and mechanical strength, carbon-based nanomaterials are frequently used in printable inks[57,58]. In this review, we discuss the contribution of carbon-family nanomaterials (CFNs), such as graphene, graphene oxide (GO), and carbon nanotubes (CNTs), in bioink formulation and their biomedical applications for tissue regeneration.

2. CFNs in biomedical applications

CFNs, composed of carbon elements, represent various spatial arrangements, such as zero-dimensional carbon quantum dots, nanodiamonds, fullerenes, one-dimensional CNTs, nanofibers, nanowires, two-dimensional (2D) graphene nanosheets, and 3D networks or their bulk counterparts[59-63]. Their carbon atoms are organized in a cubic or hexagonal lattice following sp^2 or sp^3 hybridization in conventional allotropes, including diamond and graphite[64,65]. Since the discovery of fullerenes (1985), CNTs (1991), and graphene (2004), CFNs have been extensively researched on in recent decades[66-68]. CNTs are widely used in various fields, including energy production and storage, material science, environmental sciences, as well as biomedical sciences, owing to their unique properties (small size, large surface area, and ultrathin thickness)[69-75]. When the colloidal stability of CFNs in aqueous suspensions is poor, the surface of the material is modified using covalent and non-covalent functionalization techniques, such as oxidation, dehydrogenation, plasma treatments, and ozonolysis[76,77]. Oxidized carbon nanomaterials may have 5% to 50% oxygen content depending on the synthetic procedures, thus making them water-dispersible when used in several biological applications, including TE and tissue regeneration[78], as shown in Figure 2. Carbon nanomaterials like GO and CNTs have been reported to exhibit superior optical absorption and near-infrared (NIR) conversion properties[79]. The supramolecular π–π stacking in the structure enables them to adsorb a large amount of drug, while their tunable surface chemistry enables them to control drug release[80-82]. Yin *et al.* formulated a multi-functionalized monolayer GO composite to deliver small interfering RNAs to target pancreatic cancer cells MIA PaCa-2. The tumor volume was reduced by more than 80% with the synergistic combination of gene silencing and NIR light thermotherapy of the composite[83]. Various electrochemical sensors and label-free CFNs-based biosensors have also been developed in consideration of their remarkable electronic properties[84]. In a study, a composite of antibodies-grafted CNTs was used as an immunosensor for detecting adiponectin, an obesity biomarker. Cyclic voltammetry was used to monitor the reaction of secondary antibodies conjugated with horseradish peroxidase-streptavidin with adiponectin and to quantify them, thus enabling fast detection[85].

The introduction of CFNs into soft materials, such as hydrogels, enhances the functional properties of the resulting 3D multicomponent systems; the features of CFNs-containing hydrogels meet the requirements of the promising strategies, which makes them advanced biomaterials in biomedical research[78,86]. Hossein *et al.* have reported that CNT-loaded nanocomposite hydrogels

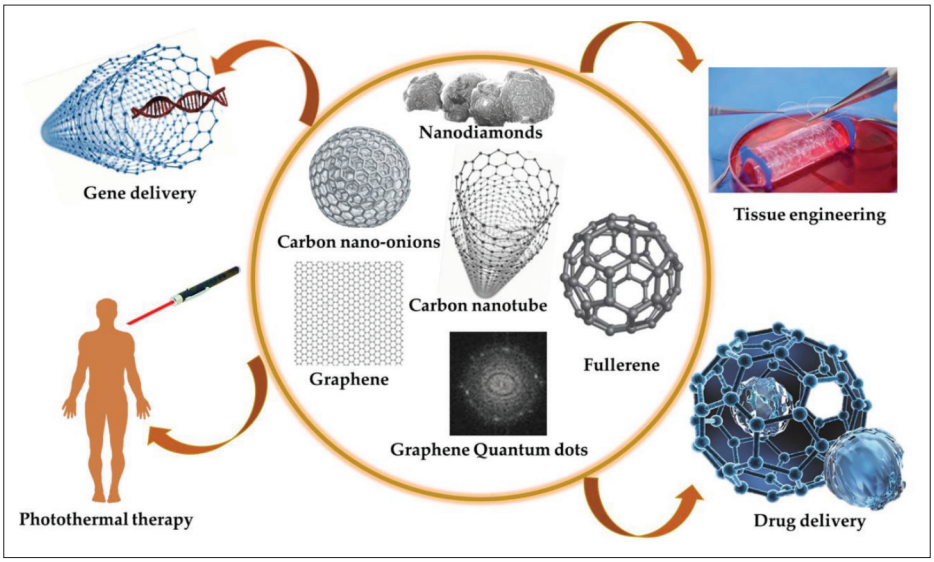

Figure 2. Various biomedical applications of carbon-family nanomaterials. Reprinted from *C*, 7, Mahor A, Singh PP, Bharadwaj P, *et al*., Carbon-based nanomaterials for delivery of biologicals and therapeutics: A cutting-edge technology, 19, Copyright (2021), with permission from MDPI[64].

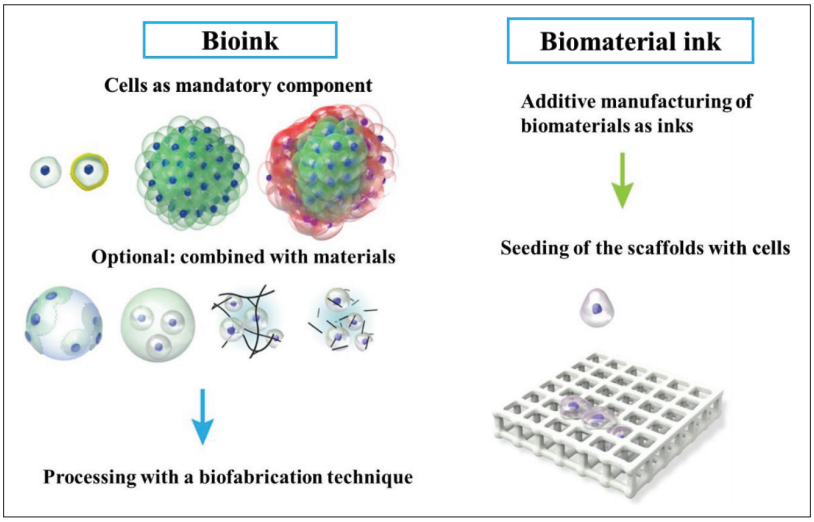

Figure 3. Difference between bioink and biomaterial ink. In bioink, cells are compulsory components of the printing formulation in the form of single cells/coated cells/cell aggregates or combinations with materials. In biomaterial ink, cells are treated with the tissue construct only after bioprinting and post-printing treatments. Reprinted from *Biofabrication*, 11, Groll J, Burdick JA, Cho DW, *et al*., A definition of bioinks and their distinction from biomaterial inks, 013001, Copyright (2018), with permission from IOP Publishing[90].

promote cell adhesion and cell migration owing to the chemoattractant properties of CNTs[87]. Following the preparation of a composite hydrogel of GO and polyacrylamide, Hyerim *et al.* investigated the composite hydrogel's capacity for skeletal muscle regeneration. They have established that graphene-incorporated electroconductive hydrogels upregulate myogenic gene expression in myoblasts via cellular interactions with electrical and mechanical signals[88]. However, it is challenging to develop robust nanocomposite hydrogels for both bioprinting and cell seeding. Li *et al.* described that the specifications of a candidate hydrogel for printing should include the characteristics of the bioinks for printing and the bioink constructs for the desired TE applications[89].

3. Combining CFNs and 3D bioprinting

Following the compilation of recently publications on CFNs incorporated in printable gel for applications in TE and tissue regeneration, we also outline the contribution of CFNs in printable gel in this review. The printable gel used for TE has been classified as a biomaterial ink and bioink, as shown in Figure 3[90]. Biomaterial inks are 3D printed and sterilized before cell seeding for application.

As biomaterial inks do not have cells, they can be subjected to post-printing treatments, such as washing, crosslinking, and UV curing, to make them stronger and biocompatible before cell line studies. In contrast, bioinks possess cells with various bioactive components and biomaterials before bioprinting. Hence, the components and crosslinking agents involved in bioinks should be biocompatible[91]. Bioinks used in 3D bioprinting can be categorized into two types: scaffold-free cell-based and cell-scaffold-based approaches for the creation of tissue- and organ-like structures. In the scaffold-free cell-based approach, living cells are printed directly to form neo-tissues and fused into the native functional tissue structures over time. In the cell-scaffold-based approach, living cells and biomaterials are mixed as bioinks; the encapsulated cells migrate and proliferate to fill the space to form a desired tissue structure in the scaffold matrix[92].

A successful bioink with suitable biomechanical properties can provide structural integrity of the printed tissue until the neo-cellular architecture begins functioning. According to Bhattacharyya *et al*., the bioink formulation must meet the following criteria: (1) the cells to be printed should be selected based on their viability during *in vitro* and *in vivo* measurements; (2) the polymer matrix or the additives incorporated into the polymeric composite should be biocompatible, and the additives should be bioactive to enhance the physicochemical and mechanical properties as well as the biofunctionalities of the printed gel; (3) the cross-linkage conditions should be amicable without stressing the printed cells, and they should not affect the cell survival rate after crosslinking; (4) the bioink layers should be able to maintain structural stability in the cell culture medium for a long time[93]. In the subsequent sections, we discuss the various CFNs-containing biomaterial inks and CFNs-containing bioinks, along with the CFNs' dimensions utilized, the specification of bioprinters, and the biological outcomes in various TE applications, as shown in Tables 1[94-103] and 2[97, 104-108], respectively.

3.1. CFNs-containing biomaterial ink

3.1.1. Graphene and carbon nanotubes in biomaterial ink

Graphene-family nanomaterials- and CNTs-incorporated printed gels have drawn considerable attention in TE owing to their excellent mechanical properties and high electrical conductivity. Large bone defects caused by external injury, infections, tumor resection, bone resorption, and nonunion fractures are treated with autologous or allogeneic bone grafts. However, these treatments have certain drawbacks, including insufficient graft quantity, donor site morbidity, and contamination. Currently, bone tissue engineering (BTE) is considered an alternative to bone grafting in replacing damaged bones using biomaterials[109-111]. Literature reports have revealed that about 2.2 million patients worldwide undergo bone grafting each year[112]. Hence, 3D bioprinting of bone tissue is regarded a rapidly evolving technology in this field. In a study, Liu *et al*. prepared a poly(propylene fumarate) (PPF)-based 3D-printed hydrogel incorporating two types of 2D materials—GO and black phosphorous (BP) nanosheets—and examined the synergistic effect of these materials on osteogenesis for BTE[94]. They used PBB (3D VIPER si2 Stereolithography System) to construct the 3D scaffold with orthogonal cubic lattice disks and square pores. Besides, they subjected the tissue construct to post-printing treatments such as washing with acetone and ethanol as well as UV curing for 2 hours to ascertain the biocompatibility and stability of the scaffold. GO nanosheets have been found to enhance cell adherence and protein adsorption in view of their large surface area, whereas GO layers-wrapped BP nanosheets continuously released phosphate ions to the medium through slow oxidation, thus facilitating MC3T3 osteoblast differentiation. Immunofluorescence assay revealed that the 3D PPF-Amine-GO@BP scaffold had a higher cell density on the surface when compared to the 3D PPF-Amine-GO, 3D PPF-Amine-BP, and 3D PPF-Amine scaffolds. The biomineralization and osteogenic differentiation results indicated that the BP anchored on the GO surface synergistically stimulated cell proliferation and osteogenesis, suggesting that the scaffold has the capacity for bone tissue regeneration.

Cartilage is formed by chondrocytes, which have poor regenerative capacity and lack extracellular matrix vascularization. Hence, treating injuries to the cartilage can be challenging[113]. Olate-Moya *et al*. have developed bioconjugated hydrogel-based nanocomposite inks that contain alginate, gelatin, chondroitin sulfate, and GO to fabricate 3D-printed scaffolds through the microextrusion process in EBB for cartilage TE[95]. After printing, the alginate chains in the extruded ink were physically crosslinked with 100 mM calcium chloride ($CaCl_2$) solution and gelatin chains via a thermotropic process. Then, the scaffolds were crosslinked with methacrylated polymers via UV irradiation (365 nm and 9 mW/cm^2). The nanofiller GO enhanced the 3D printability of bioink owing to a faster viscosity recovery during ink extrusion. Due to the templating of the GO liquid crystal, the nanocomposite inks produced anisotropic threads. The bioconjugated scaffolds displayed higher cell proliferation rate than pristine alginate, as revealed by the proliferation assay of human adipose tissue-derived MSCs (hADMSCs). Furthermore, the immunostaining assay revealed that the

Table 1. List of CFNs-containing biomaterial inks for different tissue engineering applications

CFNs and dimensions	CFNs-containing biomaterial ink	Bioprinters, crosslinking mechanisms, and scaffold's dimensions	In vitro	Biological outcomes/ tissue engineering application	Ref.
GO (synthesized by the Hummers' method; single layer sheet with a height of 1 nm)	3D-PPF-Amine, 3D-PPF-Amine-BP, 3D-PPF-Amine-GO, 3D-PPF-Amine-GO@BP	PBB (VIPER si2 Stereolithography System, Valencia, CA) Photoinitiation by BAPO Orthogonal cubic lattice disks: 5 mm × 5 mm × 5 mm (L × W × H)	MC3T3 mouse pre-osteoblast cells (30×10^3 cells/ well)	3D-PPF-Amine-GO and 3D-PPF-Amine-GO@BP promoted significant cell proliferation and osteogenesis compared to 3D-PPF-Amine and 3D-PPF-Amine-BP. Bone tissue engineering	[94]
Few-layered GO (Hummers' method; LT = 0.71 nm, LS = 1 μm)	ACG, ACG/GO0.1, and ACG/GO1	EBB (Fourth Generation 3D Bioplotter, Envision-TEC, Germany) Ca^{2+} ionic cross linkage, thermal transition, and photoinitiation by Irgacure 2959 Printed scaffold discs: 30 × 30 × 1 mm^3 (L × W × H)	hADMSCs (9.4×10^4 cells/ scaffold)	ACG/GO0.1 demonstrated greater cytocompatibility and hADMSCs differentiation. Cartilage tissue engineering	[95]
SWCNTs (Carbon Solution, Riverside, CA, USA)	NFC/alginate and NFC/alginate – 10% and 20% SWCNTs	EBB (INKREDIBLE + Bioplotter, Cellink AB, Sweden) Ca^{2+} ionic interaction Brain-slice-like construct	SH-SY5Y human neuroblastoma cells	The 10% CNTs construct had many viable cells, whereas the more conductive 20% CNTs scaffold had no attached living cells. RT-qPCR analysis showed that the 10% CNTs expressed a significant level of mature neuron marker TUBB3, compared to NFC/alginate after 10 days of incubation. Neural tissue engineering	[96]
MWCNTs (D = 10–20 nm; L = 5–50 μm)	ABT, ABT-CNT3 (0.098 g), ABT-CNT7.5 (0.244 g), and ABT-CNT10 (0.325 g)	EBB (in-house built at SeoulTech, Korea) Tannic acid and Ca^{2+} interaction, and $NaIO_4$ oxidation Disk-shaped construct (diameter = 0.5 cm; thickness = 0.2 cm)	hMSCs (0.01×10^6 cells/ well)	All the scaffolds showed cytocompatibility with hMSCs cells up to 28 days of investigation. Soft wearable bioelectronics and tissue engineering	[97]
MWCNTs (D = 80 nm; L = 10 μm) (Sigma Aldrich, USA)	PIC and PIC/MWCNTs	EBB Photoinitiation by 2-oxoglutaric acid Printed construct: 5 mm × 5 mm × 5 mm	rBMSCs (5×10^5 cells/ well)	PIC/MWCNTs demonstrated good biocompatibility with rBMSCs (days 3, 5, and 7) and favored mineralized matrix formation as well as osteogenesis-related gene upregulation (days 14 and 17), showing a significant difference compared with PIC.	[98]
			8-week-old male; 3 groups, calvarial defect model of Sprague-Dawley rats	PIC/MWCNTs promoted neovascularization and bone formation. Bone tissue engineering	

Table 1. Continued

CFNs and dimensions	CFNs-containing biomaterial ink	Bioprinters, crosslinking mechanisms, and scaffold's dimensions	In vitro	Biological outcomes/ tissue engineering application	Ref.
Amine functionalized MWCNTs (purchased from Cheap Tubes Inc.; outer diameter = 15–37 nm; L = 1–1,000 nm)	PEGDA and PEGDA-MWCNTs (MWCNTs: 0.02, 0.05, and 0.1 wt%)	PBB (Printrbot® rapid prototyping) Ultrasonication (20 KHz, 1 hour) Circular disks (diameter = 10 mm)	NSCs (30×10^3 cells/ well)	PEGDA-MWCNTs (0.1 wt%) enhanced neural stem cell proliferation and early neuronal differentiation compared to other composites after 7 days of culture. Nerve tissue regeneration	[99]
CNTs (obtained from the Institute of Process Engineering, Chinese Academy of Sciences)	Gel-SA and Gel-SA-CNTs (CNTs: 0.5 and 1%, w/v) (Gel-SA-gelatin- sodium alginate)	EBB (Regenovo Bio-Architect Pro, China) Ca^{2+} ionic cross linkage Tubular scaffold (inner diameter = 3.0 mm, outer diameter = 4.0 mm, length = 7–10 cm, wall thickness = 0.5 mm)	BALB/c skin fibroblasts (4×10^5 cells/mL)	Gel-SA and Gel-SA-CNTs (0.5%) had good cell viability and cell adhesion rate compared to Gel-SA-CNTs (1%). Vascular tissue engineering	[100]
ssDNA@CNTs (2–10 nm) (Sigma Aldrich, Milwaukee, WI)	3D-PPF, 3D-PPF-ssDNA, 3D-PPF-CNT, and 3D-PPF-ssDNA@CNTs (CNTs: 0.5 mg/mL)	PBB (VIPER si2 Stereolithography System, Valencia, CA) Photoinitiation by BAPO Orthogonal cubic-lattice disks: 5 mm × 5 mm × 5 mm (W × L × H)	MC3T3 cells (40×10^3 cells/well)	3D-PPF-ssDNA@CNTs significantly improved cell adhesion and cell spreading under electric stimulation compared to other scaffolds. Bone tissue engineering	[101]
CNFs (D = 100 nm; L = 20–200 μm) (Sigma-Aldrich, Ireland)	Alg-Gel-CNFs (CNFs: 0, 0.5, 1, 2, and 5% w/v) (Alg-Gel-alginate-gelatin)	EBB (Allevi 2 Printer, USA) Ca^{2+} ionic cross linkage Circular disks (height = 4 mm; width = 9 mm)	NIH-3T3 mouse embryonic fibroblasts (0.04×10^6 cells/ construct)	The presence of the CNFs in hydrogels did not trigger any cytotoxic effect on cultured cells for 96 hours. Meanwhile, CNFs did not significantly affect the proliferation rate of cells. Cardiac or neuronal tissue engineering	[102]
Carbonaceous material (CM) derived from algae-based biomass (prepared by the hydrothermal carbonization method, surface area 24.19 m^2/g)	PCL, CM-03/PCL, and CM-03K/PCL	EBB (Bioplotter Starter Series, EnvisionTEC) Simple dissolution in dichloromethane Printed scaffold (15 mm × 5 mm × 0.5 mm) 15 mm × 5 mm × 0.5 mm (L × W × H)	C2C12 mouse myoblasts (1×10^5 cells/scaffold)	The CM-03/PCL scaffolds significantly enhanced myotube formation and myotube maturity after electrical stimulation compared to PCL and CM-03K/PCL groups. Skeletal muscle engineering	[103]

Abbreviations: ABT, Alginate-tannic acid-bovine serum albumin; ACG, methacrylated alginate + methacrylated chondroitin sulfate + methacrylated gelatin; BAPO, bis-acylphosphine oxide; BP, black phosphorous; CNFs, carbon nanofibers; D, diameter; hADMSCs, human adipose tissue-derived mesenchymal stem cells; hMSCs, human mesenchymal stem cells; Irgacure 2959, 2-hydroxy-4′-(2-hydroxyethoxy)-2-methylpropiophenone; L × W × H, length × width × height; LS, lateral size; LT, lateral thickness; $NaIO_4$, sodium periodate; NFC, nanofibrillated cellulose; NSCs, neural stem cells; PCL, poly(ε-caprolactone); PEGDA-poly(ethylene glycol) diacrylate; PIC, polyion complex; PPF, poly(propylene fumarate); rBMSCs, rat bone marrow mesenchymal stem cells; RT-qPCR, quantitative reverse transcription polymerase chain reaction; ssDNA, single-stranded deoxyribonucleic acid; TUBB3, tubulin beta 3 class III.

Table 2. List of CFNs-containing cell-laden bioinks for different tissue engineering applications

CFNs and dimensions	Cell-laden bioink composites	Bioprinters, crosslinking mechanisms, and scaffold's dimensions	Biological outcomes/ tissue engineering application	Ref.
GO (Hummers' method; LS = 4 μm) Multilayered pluronic-stabilized graphene, G-P (physical exfoliation method; LS = 2 μm)	PU, PU/GO 25 ppm, and PU/G-P 25 ppm NSCs (4×10^6 cells/mL)	EBB (Regenovo 3D Bioprinter, China) Sol-gel thermal transition near 37°C Printed construct: 15 mm × 15 mm × 5 mm (L × W × H)	An increase in oxygen metabolism and neural differentiation of the NSCs was observed at 25 ppm of GO or G-P. Neural tissue engineering	[104]
GO (obtained from Antopaar, S. Korea, hydrodynamic diameter = 2.711 μm; BET surface area = 10.426 m^2/g)	SB, 0.25% SGOB1, 2.5% SGOB1, 3.5% SGOB1, and 0.25% SGOB2 Neuro2a mouse neuroblastoma (1×10^7 cells/ mL)	PBB (Digital Light Processing Bioprinter, NBRTech Co., Ltd., Chuncheon South Korea) Methacrylation, carbodiimidation, and photoinitiation by LAP 3D square structure: 5 mm × 5 mm × 2 mm (L × W × H)	SGOB1 bioink demonstrated larger electroconductive and mechanical behavior and significant Neuro2a cell proliferation and cell viability compared to SB. Neural tissue engineering	[105]
GO (sheet diameter < 10 μm) (Sigma Aldrich, USA)	GHPA and GO-GHPA C2C12 skeletal myoblasts (1 or 5×10^5 cells/ mL)	EBB (IINVIVO, Rokit, Seoul, Korea) Enzymatic reaction by HRP and glucose oxidase Lattice cuboid 3D model: 2 cm × 2 cm × 0.2 cm (L × W × H)	With GO in the gel, there was higher cell proliferation after 7 days of culture and more myogenic differentiation than the gel without GO. Muscle tissue engineering	[106]
GO (obtained from ANFF, University of Wollongong, Australia; average diameter = 1–2 μm, single layer sheet with a thickness of 0.81 nm)	GelMA, GelMA/GO (GO: 0.02, 0.40, and 1.40 mg/mL) PC-12 rat pheochromocytoma cell line (5×10^4 cells/mL)	EBB (CELLINK Life Sciences, Victoria, AUS) Photoinitiation by LAP Cylinder structure (diameter = 4 mm; height = 2 mm)	GelMA/GO (0.40 and 1.40 mg/mL) demonstrated an increased metabolic activity compared to GelMA and GelMA/GO (0.02 mg/mL) on day 7 of culture. Neural tissue engineering	[107]
Carboxyl group functionalized MWCNTs (D = 30 nm; L = 5–20 μm) (NanoLab, Inc., Waltham, MA)	MeCol and CNT-MeCol HCAECs ($0.8–1 \times 10^6$ cells/mL)	EBB (PolyJet Technology, Connex500, Vaughan, Ontario, Canada) Photoinitiation by Irgacure and $CaCl_2$ ionic cross linkage Printed scaffold: 8 mm × 8 mm × 2 mm (L × W × H)	HCAECs showed cellular proliferation and lumen-like formation over 10 days of treatment. Myocardial tissue engineering	[108]
MWCNTs (D = 10–20 nm; L = 5–50 μm)	ABT, ABT-CNT3 (0.098 g), ABT-CNT7.5 (0.244 g), and ABT-CNT10 (0.325 g) MC3T3 or NIH3T3 cells (0.02×10^6 cells/mL)	EBB (in-house built at SeoulTech, Korea) Tannic acid and Ca^{2+} interaction, and $NaIO_4$ oxidation Disk-shaped construct (diameter = 0.5 cm; thickness = 0.2 cm)	All the scaffolds demonstrated biocompatibility in MC3T3 and NIH3T3 cells up to 21 days of investigation. Soft wearable bioelectronics and tissue engineering	[97]

Abbreviations: ABT, alginate-tannic acid-bovine serum albumin; BET, Brunauer, Emmett, and Teller; GelMA, methacrylated gelatin; GHPA, hydroxy phenyl propionic acid conjugated gelatin; HCAECs, human coronary artery endothelial cells; HRP, horseradish peroxidase; L × W × H, length × width × height; LAP, lithium phenyl-2,4,6-trimethylbenzoylphosphinate; MeCol, methacrylated collagen; PU, polyurethane; SB, silk fibroin bioink; SGOB, silk graphene oxide bioink.

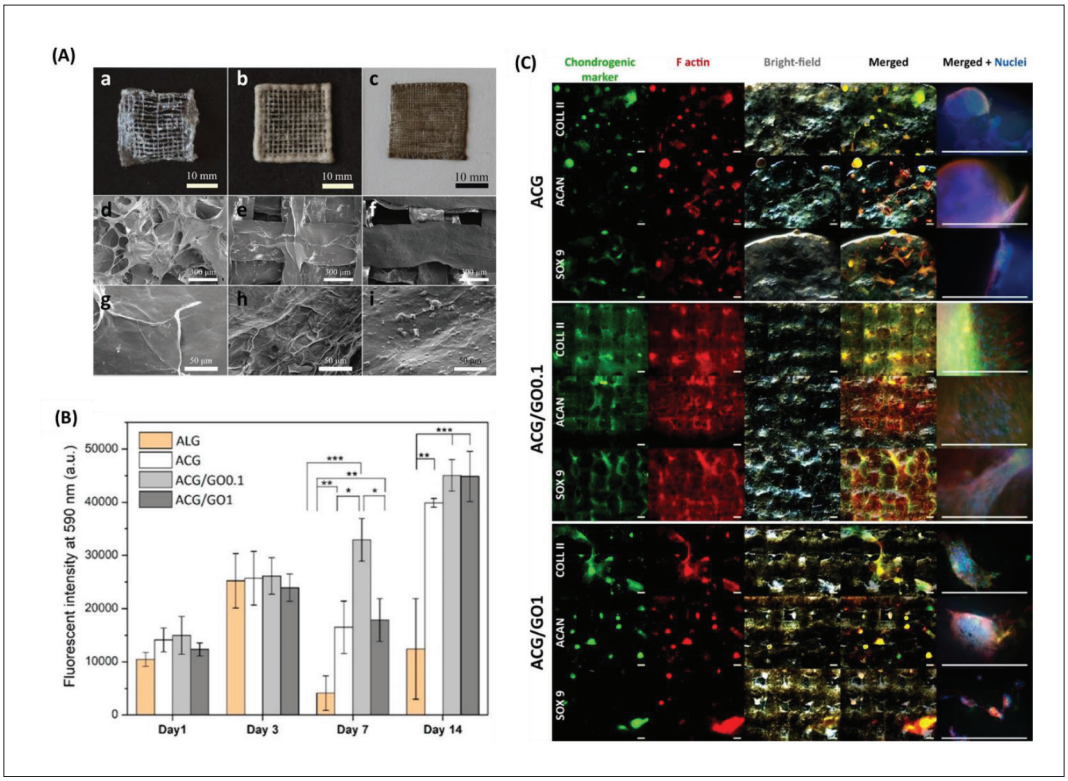

Figure 4. Chondroinductive graphene oxide (GO) containing alginate-based hydrogels (ACG). (A) Digital images of lyophilized three-dimensional (3D)-printed scaffolds of (a) ACG, (b) ACG/GO0.1, and (c) ACG/GO1. Field emission scanning electron microscopy (FE-SEM) images of their surfaces: (d, g) ACG, (e, h) ACG/GO0.1, and (f, i) ACG/GO1. (B) Proliferation of human adipose-derived mesenchymal stem cells (hADMSCs) on the printed scaffolds (*$p < 0.05$, **$p < 0.01$, and ***$p < 0.001$). (C) Immunocytochemical analysis of the chondrogenic markers (green), including collagen type II (COLL II), aggrecan (ACAN), and SOX 9, on the scaffolds after 28 days of culture. Red and blue staining indicates cytoskeleton F-actin and nuclei, respectively (scale bar: 500 μm). Reprinted from *ACS Applied Materials & Interfaces*, 12, Olate-Moya F, Arens L, Wilhelm M, *et al.*, Chondroinductive alginate-based hydrogels having graphene oxide for 3D printed scaffold fabrication, 4343–57, Copyright (2018), with permission from American Chemical Society[95].

bioconjugated gel induced chondrogenic differentiation without any additional pro-chondrogenic factors 28 days after cultivation (Figure 4).

Unlike bone and cartilage tissues, the fabrication of neural tissue through 3D bioprinting is intricate and requires excellent resolution. In a study, Bordoni *et al.* prepared a nanofibrillated cellulose (NFC)-alginate-single-walled CNTs (SWCNTs)-based 3D-printed conductive scaffold for neural TE[96]. They bioprinted the scaffold into a gelatin supporting bath following the EBB process using INKREDIBLE + Bioplotter, and then placed the scaffold in a petri dish at 37°C for 60 minutes. The human neuroblastoma cells (SH-SY5Y) cultivated on NFC/10% CNTs with differentiation factors created a complex neural network connecting the neurons within 10 days. Moreover, the cells grown on the NFC scaffold showed a typical undifferentiated cancer cell type that generates colonies; furthermore, the cells did not have any neurites. In contrast, the 10% CNTs films demonstrated differentiated cells with numerous long neurites of approximately 150 μm. In another study, Janarthanan *et al.* fabricated a proteoglycan-like gel from a bioinspired conjugate with alginate-bovine serum albumin-tannic acid (ABT) for direct four-axis printing of hollow porous tube-mimicking structures without any supporting materials[97]. The gel-loaded syringes were attached to the pneumatic-based EBB printer with multiple syringe holders for 3D printing. The $CaCl_2$ + sodium periodate ($NaIO_4$) mixture with 1 hour incubation was used for the post-printing treatment of the scaffolds. The gel became electroconductive by incorporating CNTs and 3D printable by the controlled crosslinking mechanisms of Ca^{2+} ionic interaction and $NaIO_4$ oxidation. CNTs with concentrations of 0.098, 0.244, and 0.325 g were blended into 3.25 mL of the ABT gel, and the obtained gels were labeled as ABT-CNT3, ABT-CNT7.5, and ABT-CNT10, respectively. When assessing the biocompatibility of the gels with hMSCs, the cells grown on ABT and ABT-CNT showed significantly higher cell viability than the control (latex) ($p < 0.05$), thus proving their cytocompatibility.

Cui *et al.* synthesized a tough polyion complex (PIC) hydrogel incorporating multiwall CNTs (MWCNTs) and

developed it into a 3D scaffold using extrusion-based 3D printing pneumatically for BTE[98]. According to the *in vitro* results, the 3D PIC/MWCNTs scaffolds showed excellent cytocompatibility with rat bone marrow-derived MSCs (rBMSCs). In addition, the PIC/MWCNTs scaffolds facilitated osteogenic differentiation of rBMSCs, with increased osteogenesis-related gene upregulation and mineralized matrix formation compared to PIC scaffolds. A rat calvarial defect model was used to investigate the bone tissue regeneration potential of the prepared scaffolds (PIC and PIC/MWCNTs) *in vivo*. Micro-computer tomography analysis revealed that bone regeneration occurred between 2 and 8 weeks after implantation in both scaffolds. However, the PIC/MWCNTs exceeded the PIC in terms of bone mineral density and bone volume/total volume ratio. Lee *et al*. investigated the proliferative capacity and differential potential of neural stem cells (NSCs) after seeding on amine-functionalized MWCNTs-incorporated 3D-printed scaffolds of PEG diacrylate (PEGDA)[99]. A stereolithography-based 3D PBB bioprinter was employed to fabricate neural scaffolds with intricate microarchitectures and a tunable porous structure. When the scaffolds were subjected to biphasic pulse stimulation with a 500 μA current, they significantly stimulated NSC proliferation, early neuronal differentiation, and neuronal maturity. The research concluded that an electroconductive MWCNTs-based scaffold combined with electrical stimulation (ES) synergistically enhanced neurite outgrowth in nerve tissue regeneration.

Li *et al*. fabricated cylindrical large-sized blood vessels using a hybrid bioink containing gelatin, sodium alginate, and CNTs through a combination of perpendicular directional extrusion of the printing nozzle (EBB type) and axial rotary motion of the stepper motor module[100]. Murine epidermal fibroblasts harvested from the skins of BALB/c rats were inoculated into the inner wall (3 mm) and outer wall (0.5 mm) of a hollow tubular scaffold to imitate the vascular construct. The *in vitro* study demonstrated that the doping of CNTs to the scaffold reinforced its mechanical strength and electrical conductivity, but the scaffold exhibited poor cell affinity. Liu *et al*. prepared water-dispersible negatively charged single-stranded deoxyribonucleic acid-stabilized CNTs nanocomplex (ssDNA@CNTs) and incorporated them into a 3D-printed scaffold composed of amine-functionalized PPF for bone tissue regeneration[101]. The VIPER si2 Stereolithography System based on PBB equipped with a 365 nm UV laser was used to print the scaffold. The homogenous dispersion of the nanocomplex in the scaffold enhanced cell adhesion and proliferation as well as modulated cell behavior under ES. The various fabricated scaffolds (3D-PPF, 3D-PPF-ssDNA, 3D-PPF-CNTs, and 3D-PPF-ssDNA@CNTs) expressed osteogenic differentiation markers, including alkaline phosphatase, osteocalcin, and osteopontin, in conjunction with ES, as compared with the activity of the scaffolds without ES on day 14 of culture.

3.1.2. Other CFNs in biomaterial ink

Apart from graphene and CNTs, other CFNs have also been explored for 3D printing formulations. Serafin *et al*. reinforced an alginate/gelatin (Alg–Gel) hydrogel with commercially available carbon nanofibers (CNFs; 100 nm in diameter and 20–200 μm in length) for applications in cardiac or neuronal TE[102]. The tissue construct fabricated by EBB contained two layers (2 mm per layer) with a height of 4 mm and a width of 9 mm. It was crosslinked in 200 mM $CaCl_2$ solution over 24 hours. The researchers investigated the mechanical properties, shear-thinning behavior, and electrical conductivity of the printable Alg–Gel scaffolds by using different concentrations of CNFs (0.5%, 1%, 2%, and 5% [w/v]). Incorporating CNFs into the Alg–Gel system increases the viscosity of the scaffold, thus allowing for improved ink extrusion. While optimizing the printability of the gels, all the scaffolds, except for Alg–Gel–CNFs-5, were printed successfully. Although the shape of Alg–Gel–CNFs-5 scaffold was not affected, there were multiple breakages in the printed lines. The biocompatibility study using NIH-3T3 cells demonstrated that the proliferation of the cells at 96 hours was higher for the Alg–Gel–CNFs-0 group (110.43 ± 56.5%), followed by Alg–Gel–CNFs-0.5 (82.83 ± 23.9%).

Skeletal muscle contains highly oriented and densely packed myofibrils that are mechanically and electrically active[114]. When injury occurs, the tissue's self-regeneration capacity may be limited in the case of volumetric loss. Although conventional therapeutic approaches have been developed to enhance the capacity, 3D bioprinting has been found to be effective in recapitulating the native microenvironment of tissues with a parallel-aligned structure that induces biophysical signals. In a study, Bilge *et al*. synthesized carbonaceous materials derived from algae-based biomass via hydrothermal carbonization and blended them (2% w/v) within a polycaprolactone (PCL) matrix in dichloromethane (70% w/v). They then developed 3D-printed scaffolds with dimensions of 15 mm × 5 mm × 0.5 mm using an EBB printer for skeletal muscle TE[103]. Murine C2C12 myoblasts were incubated on the electroactive scaffolds and electrically stimulated during the culture period. The electroactive scaffold groups promoted enhanced myotube formation following electrical stimulation compared with their non-conductive

counterparts, suggesting that electrical cues have major roles in the differentiation of myoblasts.

3.2. CFNs-containing bioink

Huang *et al.* developed a graphene-based nanocomposite hydrogel for neural TE by mixing water-dispersible graphene (Pluronic stabilized, G-P) and GO with polyurethane (PU)[104]. NSCs-embedded gel was extruded using a commercial EBB bioprinter, and the constructs were then added to the cell culture medium while maintaining it at 37°C. The addition of graphene nanomaterials (25 ppm) to NSCs (4×10^6 cells/mL)-embedded composite (PU/G-P 25 ppm or PU/GO 25 ppm) significantly increased adenosine triphosphate production and oxygen metabolism in cells by approximately two- to fourfold compared to PU hydrogel after 24 hours of culture. The NSCs-treated PU/G-P 25 ppm scaffold showed an increased gene expression of the glial fibrillary acidic protein and β-tubulin after 3 days of culture by factors of 5.5 and 1.5, respectively, as compared to those of PU and PU/GO 25 ppm scaffolds. The synthesized hydrogel composite system containing thermoresponsive PU and graphene met both, the mechanical requirements of bioprinted scaffolds and the biological requirements for stimulating the differentiation of NSCs. Ajiteru *et al.* formulated a bioink using glycidyl methacrylated silk fibroin (SB) with covalently reduced GO and fabricated a tissue construct (SGOB) using a customized digital light processing printer (PBB type). The fabricated scaffold exhibited enhanced electroconductive, mechanical, and neurogenic properties, as compared to SB alone, and the photocurable bioink containing Neuro2a neuroblastoma (1×10^7 cells/mL) enhanced cell viability and proliferation, thus proving its suitability as a biocomposite for neural TE[105].

Additionally, we have fabricated a 3D-printable bioink that is combined with phenol-rich gelatin (GHPA), GO, and C2C12 myoblasts via a dual enzyme-mediated crosslinking reaction (glucose oxidase and horseradish peroxidase) for skeletal muscle TE[106]. The 3D-printed construct obtained via EBB retained its shape fidelity immediately after printing. As demonstrated in the live/dead assay, the printing process did not affect the loaded C2C12 myoblasts because most cells exhibited green fluorescence. The hydrogel (GO/GHPA) conferred a suitable cellular microenvironment that facilitated the myogenic differentiation of myoblasts. The cells spread their filopodia to adhere to the hydrogel structures on days 3 and 5 and formed a mesh-like morphology on day 7, thus denoting cell proliferation (Figure 5).

Mendes *et al.* formed a 3D-printed structure of photo-crosslinkable soft hybrid GelMA/GO using EBB. The printed structure has a greater electroactive surface area than its non-printed counterpart containing the same amount of GelMA/GO. They demonstrated that by adding a small amount of GO (<0.07% volume fraction) to the gel, the impedance significantly decreased by 35-fold, while the mechanical property increased by 2-fold compared with GelMA alone. In addition, GO increased the rheological properties of the GelMA composite, improving the printability, shape fidelity, and integrity of the 3D-printed construct. The PC-12 pheochromocytoma cells incorporated with GelMA/GO-printed gel of 0.40 and 1.40 mg/mL GO concentrations demonstrated higher metabolic activity compared to GelMA and GelMA/GO with GO concentration of 0.02 mg/mL 7 days post-treatment. These research findings have supported the use of 3D-printed GelMA/GO composite gels in electrically directed cell behavior in various types of tissue regeneration[107].

For biofabrication of cell-supportive cardiac patches, the scaffold must be mechanically elastic, robust, electrically conductive, and biologically active. Cardiac patches should imitate the myocardial extracellular matrix with the capacity for rapid integration with the native tissues[115]. Izadifar *et al.* developed a nanoreinforced methacrylated collagen–CNT hybrid cardiac patch laden with human coronary artery endothelial cells (HCAECs) with excellent mechanical, electrical, and cellular responses[108]. Compared to the CNT-free hybrid constructs, the UV-integrated (365 nm, 45 seconds) EBB-printed hybrid constructs have demonstrated much higher electrical conductivity in the frequency range (approximately 5 Hz) associated with the physiological state. The CNTs in HCAECs promoted enhanced cellular behaviors, such as migration, proliferation, and lumen-like formation, 10 days post-incubation. "Electron hopping" or "tunneling" is known to govern the electrical conductivity of CNTs by affording a continuous electron path along the CNT interconnects[116]. Janarthanan *et al.* developed an ABT bioink with the incorporation of various concentrations (0.098 g, 0.244 g, and 0.325 g) of CNTs and 0.02×10^6 cells/mL of MC3T3 osteoblasts or NIH3T3 fibroblasts. The EBB-printed disk-shaped scaffolds exhibited cell biocompatibility for up to 21 days of the investigation[97].

4. Conclusion and perspectives

The primary purpose of fabricating 3D-bioprinted constructs is to aid in TE and tissue regeneration. Although 3D bioprinting techniques demand advanced and costly infrastructures, including software, robust computer workrooms, and cell culture laboratory facilities, these techniques allow us to fabricate scaffolds with complex biological arrangements with greater shape fidelity and patient-specific designs within a short duration. In this

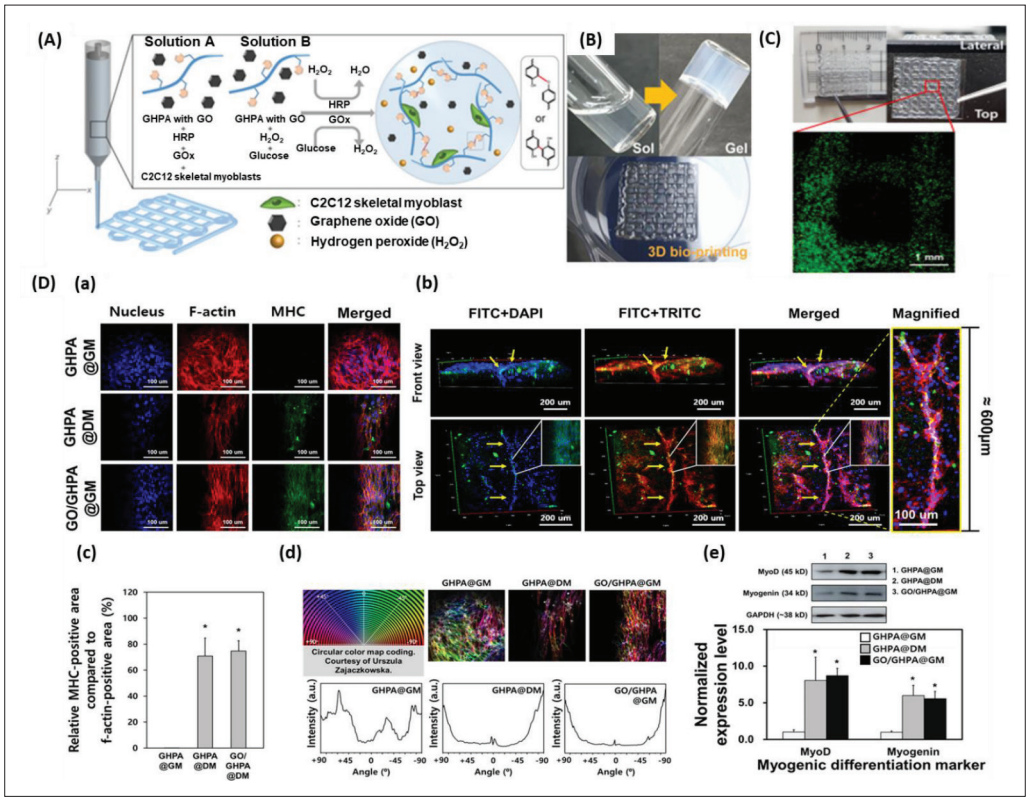

Figure 5. (A) Schematic explanation of the components and crosslinking process of graphene oxide (GO)/phenol-rich gelatin (GHPA) hydrogel formation. (B) Full size images of the sol–gel phase transition of the GO/GHPA gel and its three-dimensional (3D)-printed construct. (C) Live/dead assay of the cell-laden 3D-printed constructs. (D) Immunocytochemical analysis of C2C12 cell-laden hydrogels. (a) Confocal microscope images of the cell-laden construct cultured in GHPA@GM (GHPA hydrogel cultured in growth medium), GHPA@DM (GHPA hydrogel cultured in differentiation medium), and GO/GHPA@GM (GO/GHPA hydrogel cultured in growth medium). Fluorescein-5-isothiocyanate (FITC), tetramethylrhodamine-isothiocyanate (TRITC), and 4′,6-diamidino-2-phenylindole (DAPI) stain myosin heavy chain (MHC), f-actin, and nucleus, respectively. (b) 3D images of GO/GHPA@GM were acquired through z-stack confocal microscope imaging. (c) The ratio of MHC-positive area per cell area of the printed constructs. (d) F-actin orientation measured by color mapping. (e) Western blot and normalized expression level of myogenic markers on the C2C12 cells in printed constructs. Reprinted from *ACS Macro Letters*, 10, Kang MS, Kang JI, Le Thi P, *et al*., Three-dimensional printable gelatin hydrogels incorporating graphene oxide to enable spontaneous myogenic differentiation, 426–32, Copyright (2021), with permission from American Chemical Society[106].

review, we highlight the different types of bioprinters and list out the various CFNs-containing printable gels as biomaterial inks and cell-laden bioinks for TE applications. We also discuss the properties of CFNs and their contribution to hydrogels for various applications. We have established that CFNs in printable gel aid in cellular growth owing to their electrochemical properties; particularly, low-concentrated CFNs can potentially improve tissue regeneration more than their highly concentrated counterparts. However, we have encountered some problems that need to be addressed in future research:

(i) Graphene sheets and CNTs have been widely used in printable gels; however, the use of CFNs such as CNFs, fullerenes, and carbon quantum dots has not been extensively explored in combination with printable gels for TE. Researchers should focus on each dimensional carbon nanomaterial in printable gels, as they possess unique properties in addition to their common electrochemical properties.

(ii) There are more literature on CFNs-containing biomaterial ink than on CFNs-containing bioink. In order to select biomaterial inks that are suitable for cell-laden bioinks, various parameters that can harm viable cells, such as heating effect, solvents, number of steps, and crosslinking agents involved in the formulation of biomaterial inks, must be considered before or during printing. Hence, researchers who are involved in conducting preliminary studies on printable gels should have a good grasp of the challenges that would be encountered before formulating a bioink.

(iii) Among the bioprinting systems, only EBB printers have been widely used by researchers to execute the printing of CFNs-containing printable gels. Hence, in the

coming years, researchers should employ the underutilized bioprinters to fabricate tissue constructs.

(iv) Several researchers have utilized encapsulated CFNs, while some others have used bare nanomaterials. As the stabilization of nanoparticles plays a crucial role in biocompatibility, a comparative study employing encapsulated and non-encapsulated CFNs-containing printable gels should be conducted.

(v) Apart from electrochemical properties, CFNs have been used as fillers to improve the mechanical strength of printable gels. Researchers should attempt to prepare modified or doped CFNs with reactive groups on the surface, which can crosslink polymers and express multifunctionality during application.

(vi) Enhanced cell proliferation is the major biological outcome of the combined CFNs with printable gel. Despite the studies that have been performed on molecular level, researchers have never discussed how nanomaterials interact among themselves and with the cells in the tissue construct after fabrication. A detailed analysis of this would assist nanotechnologists in their venture of exploring more about CFNs-printable gels.

We anticipate that researchers with interdisciplinary backgrounds will advance the field of TE and regenerative medicine using CFNs-containing printable gels by considering the aforementioned problems and suggestions.

Acknowledgments

None.

Funding

This research was supported by the Basic Science Research Program through the National Research Foundation of Korea (NRF) funded by the Ministry of Education (No. 2022R1I1A1A01064416), the NRF grant funded by the Korean Government (MSIT) (Nos. 2021R1A2C2006013 and 2020R1F1A1072695), and the Ministry of Trade, Industry and Energy, Korea, under the "Regional Innovation Cluster Development Program (R&D, P0015342)" supervised by the Korea Institute for Advancement of Technology (KIAT).

Conflict of interest

The authors declare no conflicts of interest.

Author contributions

Writing – original draft: Iruthayapandi Selestin Raja, Moon Sung Kang

Writing – review & editing: Suck Won Hong, Hojae Bae, Bongju Kim, Yu-Shik Hwang

Conceptualization & revision: Jae Min Cha, Dong-Wook Han

Ethics approval and consent to participate

Not applicable.

Consent for publication

Not applicable.

Availability of data

Not applicable.

References

1. Gopinathan J, Noh I, 2018, Recent trends in bioinks for 3D printing. *Biomater Res*, 22:11.
2. Cha M, Jin YZ, Park JW, *et al*., 2021, Three-dimensional printed polylactic acid scaffold integrated with BMP-2 laden hydrogel for precise bone regeneration. *Biomater Res*, 25:35.
3. Murphy SV, Atala A, 2014, 3D bioprinting of tissues and organs. *Nat Biotechnol*, 32:773–785.
4. Guvendiren M, Molde J, Soares RMD, *et al*., 2016, Designing biomaterials for 3D printing. *ACS Biomater Sci Eng*, 2:1679–1693.
5. Kang MS, Kwon M, Lee SY, *et al*., 2022, In situ crosslinkable collagen-based hydrogels for 3D printing of dermis-mimetic constructs. *ECS J Solid State Sci Technol*, 11:045014.
6. Kang MS, Kwon M, Lee SH, *et al*., 2022, 3D printing of skin equivalents with hair follicle structures and epidermal-papillary-dermal layers using gelatin/hyaluronic acid hydrogels. *Chem Asian J*, 17: e202200620.
7. Ozbolat IT, Peng W, Ozbolat V, 2016, Application areas of 3D bioprinting. *Drug Discov Today*, 21:1257–1271.
8. Weng T, Zhang W, Xia Y, *et al*., 2021, 3D bioprinting for skin tissue engineering: Current status and perspectives. *J Tissue Eng*, 12:20417314211028574.
9. Gu Z, Fu J, Lin H, et al., 2020, Development of 3D bioprinting: From printing methods to biomedical applications. *Asian J Pharm Sci*, 15:529–557.
10. Gudapati H, Dey M, Ozbolat I, 2016, A comprehensive review on droplet-based bioprinting: Past, present and future. *Biomaterials*, 102:20–42.
11. Derby B, 2010, Inkjet printing of functional and structural materials: Fluid property requirements, feature stability, and resolution. *Annu Rev Mater Res*, 40:395–414.
12. Nakamura M, Kobayashi A, Takagi F, *et al*., 2005, Biocompatible inkjet printing technique for designed seeding of individual living cells. *Tissue Eng*, 11:1658–1666.

13. Binder KW, Zhao W, Aboushwareb T, *et al*., 2010, In situ bioprinting of the skin for burns. *J Am Coll Surg*, 211:S76.
14. Ozbolat IT, Hospodiuk M, 2016, Current advances and future perspectives in extrusion-based bioprinting. *Biomaterials*, 76:321–343.
15. Koch L, Gruene M, Unger C, *et al*., 2013, Laser assisted cell printing. *Curr Pharm Biotechnol*, 14:91–97.
16. Guillemot F, Souquet A, Catros S, *et al*., 2010, Laser-assisted cell printing: Principle, physical parameters versus cell fate and perspectives in tissue engineering. *Nanomedicine*, 5:507–515.
17. Koch L, Kuhn S, Sorg H, *et al*., 2010, Laser printing of skin cells and human stem cells. *Tissue Eng Part C Methods*, 16:847–854.
18. Serra P, Duocastella M, Fernández-Pradas JM, *et al*., 2009, Liquids microprinting through laser-induced forward transfer. *Appl Surf Sci*, 255:5342–5345.
19. Patrascioiu A, Fernández-Pradas JM, Palla-Papavlu A, *et al*., 2014, Laser-generated liquid microjets: Correlation between bubble dynamics and liquid ejection. *Microfluid Nanofluid*, 16:55–63.
20. Pan Y, Zeng L, 2019, Simulation and validation of droplet generation process for revealing three design constraints in electrohydrodynamic jet printing. *Micromachines*, 10:94.
21. Mkhize N, Bhaskaran H, 2022, Electrohydrodynamic jet printing: Introductory concepts and considerations. *Small Sci*, 2:2100073.
22. Lei Q, He J, Li D, 2019, Electrohydrodynamic 3D printing of layer-specifically oriented, multiscale conductive scaffolds for cardiac tissue engineering. *Nanoscale*, 11:15195–15205.
23. Jeong HJ, Nam H, Jang J, *et al*., 2020, 3D bioprinting strategies for the regeneration of functional tubular tissues and organs. *Bioengineering*, 7:32.
24. Dhariwala B, Hunt E, Boland T, 2004, Rapid prototyping of tissue-engineering constructs, using photopolymerizable hydrogels and stereolithography. *Tissue Eng*, 10:1316–1322.
25. Melchels FPW, Feijen J, Grijpma DW, 2010, A review on stereolithography and its applications in biomedical engineering. *Biomaterials*, 31:6121–6130.
26. Lopez de Armentia S, Fernández-Villamarín S, Ballesteros Y, *et al*., 2022, 3D printing of a graphene-modified photopolymer using stereolithography for biomedical applications: A study of the polymerization reaction. *Int J Bioprint*, 8:503.
27. Heinrich MA, Liu W, Jimenez A, *et al*., 2019, 3D bioprinting: From benches to translational applications. *Small*, 15:e1805510.
28. Moura D, Pereira RF, Gonçalves IC, 2022, Recent advances on bioprinting of hydrogels containing carbon materials. *Mater Today Chem*, 23:100617.
29. Seo JW, Kim GM, Choi Y, *et al*., 2022, Improving printability of digital-light-processing 3D bioprinting via photoabsorber pigment adjustment. *Int J Mol Sci*, 23:5428.
30. Mironov V, Boland T, Trusk T, *et al*., 2003, Organ printing: Computer-aided jet-based 3D tissue engineering. *Trends Biotechnol*, 21:157–161.
31. Shafiee A, Atala A, 2016, Printing technologies for medical applications. *Trends Mol Med*, 22:254–265.
32. Fielding GA, Bandyopadhyay A, Bose S, 2012, Effects of silica and zinc oxide doping on mechanical and biological properties of 3D printed tricalcium phosphate tissue engineering scaffolds. *Dent Mater*, 28:113–122.
33. Ahmed M, Vadivelu R, John J, *et al*., 2016, Three-dimensional printing of biological matters. *J Sci Adv Mater Devices*, 1:1–17.
34. Li Q, Zhang B, Xue Q, *et al*., 2021, A systematic thermal analysis for accurately predicting the extrusion printability of alginate–gelatin-based hydrogel bioinks. *Int J Bioprint*, 7:394.
35. Matai I, Kaur G, Seyedsalehi A, *et al*., 2020, Progress in 3D bioprinting technology for tissue/organ regenerative engineering. *Biomaterials*, 226:119536.
36. Liu W, Zhang YS, Heinrich MA, *et al*., 2017, Rapid continuous Multimaterial mxtrusion bioprinting. *Adv Mater*, 29:1604630.
37. Kreimendahl F, Köpf M, Thiebes AL, *et al*., 2017, Three-dimensional printing and angiogenesis: Tailored agarose-type I collagen blends comprise three-dimensional printability and angiogenesis potential for tissue-engineered substitutes. *Tissue Eng Part C Methods*, 23:604–615.
38. Noh I, Kim N, Tran HN, *et al*., 2019, 3D Printable hyaluronic acid-based hydrogel for its potential application as a bioink in tissue engineering. *Biomat Res*, 23:3.
39. Pereira RF, Sousa A, Barrias CC, *et al*., 2018, A single-component hydrogel bioink for bioprinting of bioengineered 3D constructs for dermal tissue engineering. *Mater Horiz*, 5:1100–1111.
40. Ashammakhi N, Ahadian S, Xu C, *et al*., 2019, Bioinks and bioprinting technologies to make heterogeneous and biomimetic tissue constructs. *Mater Today Bio*, 1:100008.
41. Suntornnond R, Tan EYS, An J, *et al*., 2017, A highly printable and biocompatible hydrogel composite for direct printing of soft and perfusable vasculature-like structures. *Sci Rep*, 7:16902.
42. Cernencu AI, Lungu A, Dragusin DM, *et al*., 2021, 3D bioprinting of biosynthetic nanocellulose-filled GelMA inks highly reliable for soft tissue-oriented constructs. *Materials*, 14:4891.
43. Pereira RF, Bártolo PJ, 2015, 3D bioprinting of photocrosslinkable hydrogel constructs. *J Appl Polym Sci*, 132:42458.
44. Escobar-Chávez JJ, López-Cervantes M, Naïk A, *et al*., 2006, Applications of thermo-reversible pluronic F-127 gels in pharmaceutical formulations. *J Pharm Sci*, 9:339–358.
45. Setayeshmehr M, Hafeez S, van Blitterswijk C, *et al*., 2021, Bioprinting via a dual-gel bioink based on poly(vinyl

alcohol) and solubilized extracellular matrix towards cartilage engineering. *Int J Mol Sci*, 22:3901.

46. Ouyang L, Highley CB, Sun W, *et al*., 2017, A generalizable strategy for the 3D bioprinting of hydrogels from nonviscous photo-crosslinkable inks. *Adv Mater*, 29:1604983.

47. Bertlein S, Brown G, Lim KS, *et al*., 2017, Thiol-ene clickable gelatin: A platform bioink for multiple 3D biofabrication technologies. *Adv Mater*, 29:1703404.

48. Wang SJ, Zhang ZZ, Jiang D, *et al*., 2016, Thermogel-coated poly(ε-caprolactone) composite scaffold for enhanced cartilage tissue engineering. *Polymers*, 8:200.

49. Zhang K, Xue K, Loh XJ, 2021, Thermo-responsive hydrogels: From recent progress to biomedical applications. *Gels*, 7:77.

50. Iglesias-Mejuto A, García-González CA, 2022, 3D-printed, dual crosslinked and sterile aerogel scaffolds for bone tissue engineering. *Polymers*, 14:1211.

51. Mora-Boza A, Włodarczyk-Biegun MK, Del Campo A, *et al*., 2019, Glycerylphytate as an ionic crosslinker for 3D printing of multi-layered scaffolds with improved shape fidelity and biological features. *Biomater Sci*, 8:506–516.

52. Olmos-Juste R, Alonso-Lerma B, Pérez-Jiménez R, *et al*., 2021, 3D printed alginate-cellulose nanofibers based patches for local curcumin administration. *Carbohydr Polym*, 264:118026.

53. Howell DW, Peak CW, Bayless KJ, *et al*., 2018, 2D nanosilicates loaded with proangiogenic factors stimulate endothelial sprouting. *Adv Biosyst*, 2:1800092.

54. Bendtsen ST, Quinnell SP, Wei M, 2017, Development of a novel alginate-polyvinyl alcohol-hydroxyapatite hydrogel for 3D bioprinting bone tissue engineered scaffolds. *J Biomed Mater Res Part A*, 105:1457–1468.

55. Bonnelye E, Chabadel A, Saltel F, *et al*., 2008, Dual effect of strontium ranelate: Stimulation of osteoblast differentiation and inhibition of osteoclast formation and resorption in vitro. *Bone*, 42:129–138.

56. Jeong WY, Kang MS, Lee H, *et al*., 2021, Recent trends in photoacoustic imaging techniques for 2D nanomaterial-based phototherapy. *Biomedicines*, 9:80.

57. Yu D, Goh K, Wang H, *et al*., 2014, Scalable synthesis of hierarchically structured carbon nanotube–graphene fibres for capacitive energy storage. *Nat Nanotechnol*, 9:555–562.

58. Rueda-Gensini L, Serna JA, Cifuentes J, *et al*., 2021, Graphene oxide-embedded extracellular matrix-derived hydrogel as a multiresponsive platform for 3D bioprinting applications. *Int J Bioprint*, 7:353.

59. Raja IS, Song SJ, Kang MS, *et al*., 2019, Toxicity of zero- and one-dimensional carbon nanomaterials. *Nanomaterials*, 9:1214.

60. Shin YC, Song SJ, Jeong SJ, *et al*., 2018, Graphene-based nanocomposites as promising options for hard tissue regeneration. *Adv Exp Med Biol*, 1078:103–117.

61. Kang MS, Song S-J, Cha JH, *et al*., 2020, Increased neuritogenesis on ternary nanofiber matrices of PLCL and laminin decorated with black phosphorus. *J Ind Eng Chem*, 92:226–235.

62. Raja IS, Kang MS, Kim KS, *et al*., 2020, Two-dimensional theranostic nanomaterials in cancer treatment: State of the art and perspectives. *Cancers*, 12:1657.

63. Raja IS, Lee JH, Hong SW, *et al*., 2021, A critical review on genotoxicity potential of low dimensional nanomaterials. *J Hazard Mater*, 409:124915.

64. Mahor A, Singh PP, Bharadwaj P, *et al*., 2021, Carbon-based nanomaterials for delivery of biologicals and therapeutics: A cutting-edge technology. *C*, 7:19.

65. Perkins BL, Naderi N, 2016, Carbon nanostructures in bone tissue engineering. *Open Orthop J*, 10:877–899.

66. Rauti R, Musto M, Bosi S, *et al*., 2019, Properties and behavior of carbon nanomaterials when interfacing neuronal cells: How far have we come? *Carbon*, 143:430–446.

67. Kang MS, Lee JH, Hong SW, *et al*., 2021, Nanocomposites for enhanced osseointegration of dental and orthopedic implants revisited: Surface functionalization by carbon nanomaterial coatings. *J Compos Sci*, 5:23.

68. Kang MS, Jang HJ, Lee SH, *et al*., 2021, Potential of carbon-based nanocomposites for dental tissue engineering and regeneration. *Materials*, 14:5104.

69. Li Q, Song J, Besenbacher F, *et al*., 2015, Two-dimensional material confined water. *Acc Chem Res*, 48:119–127.

70. Yu D, Goh K, Wang H, *et al*., 2014, Scalable synthesis of hierarchically structured carbon nanotube-graphene fibres for capacitive energy storage. *Nat Nanotechnol*, 9:555–562.

71. Liu Y, Dong X, Chen P, 2012, Biological and chemical sensors based on graphene materials. *Chem Soc Rev*, 41:2283–2307.

72. Raja IS, Vedhanayagam M, Preeth DR, *et al*., 2021, Development of two-dimensional nanomaterials based electrochemical biosensors on enhancing the analysis of food toxicants. *Int J Mol Sci*, 22:3277.

73. Shin YC, Bae J-H, Lee JH, *et al*., 2022, Enhanced osseointegration of dental implants with reduced graphene oxide coating. *Biomater Res*, 26:11.

74. Vedhanayagam M, Raja IS, Molkenova A, *et al*., 2021, Carbon dots-mediated fluorescent scaffolds: Recent trends in image-guided tissue engineering applications. *Int J Mol Sci*, 22:5378.

75. Kang MS, Lee H, Jeong S, *et al*., 2022, State of the art in carbon nanomaterials for photoacoustic imaging. *Biomedicines*, 10:1374.

76. Konios D, Stylianakis MM, Stratakis E, *et al*., 2014, Dispersion behaviour of graphene oxide and reduced graphene oxide. *J Colloid Interface Sci*, 430:108–112.

77. Li H, Song SI, Song GY, *et al*., 2014, Non-covalently functionalized carbon nanostructures for synthesizing carbon-based hybrid nanomaterials. *J Nanosci Nanotechnol*, 14:1425–1440.

78. Adorinni S, Rozhin P, Marchesan S, 2021, Smart hydrogels meet carbon nanomaterials for new frontiers in medicine. *Biomedicines*, 9:570.

79. Simon J, Flahaut E, Golzio M. 2019, Overview of carbon nanotubes for biomedical applications. *Materials*, 12:624.

80. Debnath SK, Srivastava R. 2021, Drug delivery with carbon-based nanomaterials as versatile nanocarriers: Progress and prospects. *Front Nanotechnol*, 3:644564.

81. Luo X, Matranga C, Tan S, *et al*., 2011, Carbon nanotube nanoreservior for controlled release of anti-inflammatory dexamethasone. *Biomaterials*, 32:6316–6323.

82. Chae SY, Shin MC, Jeon S, *et al*., 2021, Simple route to the complexation of lutein with reduced graphene oxide nanocarriers and antioxidant protection against blue light. *Int J Nanomed*, 16:6843–6860.

83. Yin F, Hu K, Chen Y, *et al*., 2017, SiRNA delivery with PEGylated graphene oxide nanosheets for combined photothermal and genetherapy for pancreatic cancer. *Theranostics*, 7:1133–1148.

84. Chen H, Huang J, Fam DWH, *et al*., 2016, Horizontally aligned carbon nanotube based biosensors for protein detection. *Bioengineering*, 3:23.

85. Ojeda I, Barrejón M, Arellano LM, *et al*., 2015, Grafted-double walled carbon nanotubes as electrochemical platforms for immobilization of antibodies using a metallic-complex chelating polymer: Application to the determination of adiponectin cytokine in serum, *Biosens Bioelectron*, 74:24–29.

86. Lee JH, Lee Y, Shin YC, *et al*., 2016, In situ forming gelatin/graphene oxide hydrogels for facilitated C2C12 myoblast differentiation. *Appl Spectrosc Rev*, 51:527–539.

87. Ravanbakhsh H, Bao G, Mongeau L, 2020, Carbon nanotubes promote cell migration in hydrogels. *Sci Rep*, 10: 2543.

88. Jo H, Sim M, Semin K, *et al*., 2016, Electrically conductive graphene/polyacrylamide hydrogels produced by mild chemical reduction for enhanced myoblast growth and differentiation. *Acta Biomater*, 48; 100–109.

89. Li H, Tan C, Li L, 2018, Review of 3D printable hydrogels and constructs. *Mater Des*, 159:20–38.

90. Groll J, Burdick JA, Cho DW, *et al*., 2018, A definition of bioinks and their distinction from biomaterial inks. *Biofabrication*, 11:013001.

91. Schuurman W, Khristov V, Pot MW, *et al*., 2011, Bioprinting of hybrid tissue constructs with tailorable mechanical properties. *Biofabrication*, 3:021001.

92. Kaushik SN, Kim B, Walma AM, *et al*., 2016, Biomimetic microenvironments for regenerative endodontics. *Biomater Res*, 20:14.

93. Bhattacharyya A, Janarthanan G, Noh I, 2021, Nano-biomaterials for designing functional bioinks towards complex tissue and organ regeneration in 3D bioprinting. *Addit Manuf*, 37:101639.

94. Liu X, Miller AL, Park S, *et al*., 2019, Two-dimensional black phosphorus and graphene oxide nanosheets synergistically enhance cell proliferation and osteogenesis on 3D printed scaffolds. *ACS Appl Mater Interfaces*, 11:23558–23572.

95. Olate-Moya F, Arens L, Wilhelm M, *et al*., 2020, Chondroinductive alginate-based hydrogels having graphene oxide for 3D printed scaffold fabrication. *ACS Appl Mater Interfaces*, 12:4343–4357.

96. Bordoni M, Karabulut E, Kuzmenko V, *et al*., 2020, 3D printed conductive nanocellulose scaffolds for the differentiation of human neuroblastoma cells. *Cells*, 9:682.

97. Janarthanan G, Lee S, Noh I, 2021, 3D printing of bioinspired alginate-albumin based instant gel ink with electroconductivity and its expansion to direct four-axis printing of hollow porous tubular constructs without supporting materials. *Adv Funct Mater*, 31:2104441.

98. Cui H, Yu Y, Li X, *et al*., 2019, Direct 3D printing of a tough hydrogel incorporated with carbon nanotubes for bone regeneration. *J Mater Chem B*, 7:7207–7217.

99. Lee SJ, Zhu W, Nowicki M, *et al*., 2018, 3D printing nano conductive multi-walled carbon nanotube scaffolds for nerve regeneration. *J Neural Eng*, 15:016018.

100. Li L, Qin S, Peng J, *et al*., 2020, Engineering gelatin-based alginate/carbon nanotubes blend bioink for direct 3D printing of vessel constructs. *Int J Biol Macromol*, 145:262–271.

101. Liu X, George MN, Park S, *et al*., 2020, 3D-printed scaffolds with carbon nanotubes for bone tissue engineering: Fast and homogeneous one-step functionalization. *Acta Biomater*, 111:129–140.

102. Serafin A, Murphy C, Rubio MC, *et al*., 2021, Printable alginate/gelatin hydrogel reinforced with carbon nanofibers as electrically conductive scaffolds for tissue engineering. *Mater Sci Eng C Mater Biol Appl*, 122:111927.

103. Bilge S, Ergene E, Talak E, *et al*., 2021, Recycled algae-based carbon materials as electroconductive 3D printed skeletal muscle tissue engineering scaffolds. *J Mater Sci Mater Med*, 32:73.

104. Huang CT, Kumar Shrestha L, Ariga K, *et al*., 2017, A graphene-polyurethane composite hydrogel as a potential bioink for 3D bioprinting and differentiation of neural stem cells. *J Mater Chem B*, 5:8854–8864.

105. Ajiteru O, Sultan MT, Lee YJ, *et al*., 2020, A 3D printable electroconductive biocomposite bioink based on silk fibroin-conjugated graphene oxide. *Nano Lett*, 20:6873–6883.

106. Kang MS, Kang JI, Le Thi P, *et al*., 2021, Three-dimensional printable gelatin hydrogels incorporating graphene oxide to enable spontaneous myogenic differentiation. *ACS Macro Lett*, 10:426–432.

107. Xavier Mendes A, Moraes Silva S, O'Connell CD, *et al*., 2021, Enhanced electroactivity, mechanical properties, and printability through the addition of graphene oxide to photo-cross-linkable gelatin methacryloyl hydrogel. *ACS Biomater Sci Eng*, 7:2279–2295.

108. Izadifar M, Chapman D, Babyn P, *et al*., 2018, UV-assisted 3D bioprinting of nanoreinforced hybrid cardiac patch for myocardial tissue engineering. *Tissue Eng Part C Methods*, 24:74–88.

109. Liu J, Li L, Suo H, *et al*., 2019, 3D printing of biomimetic multi-layered GelMa/nHA scaffold for osteochondral defect repair. *Materi Des*, 171:107708.

110. Gandra N, Wang DD, Zhu Y, *et al*., 2013 Virus-mimetic cytoplasm-cleavable magnetic/silica nanoclusters for enhanced gene delivery to mesenchymal stem cells. *Angew Chem*, 52:11278–11281.

111. Rudiansyah M, El-Sehrawy AA, Ahmad I, *et al*., 2022, Osteoporosis treatment by mesenchymal stromal/stem cells and their exosomes: Emphasis on signaling pathways and mechanisms. *Life Sci*, 306:120717.

112. Bhatt RA, Rozental TD, 2012, Bone graft substitutes. *Hand Clin*, 28:457–468.

113. Calikoglu Koyuncu AC, Gurel Pekozer G, Ramazanoglu M, *et al*., 2017, Cartilage tissue engineering on macroporous scaffolds using human tooth germ stem cells. *J Tissue Eng Regen Med*, 11:765–777.

114. Ito A, Yamamoto Y, Sato M, *et al*., 2014, Induction of functional tissue-engineered skeletal muscle constructs by defined electrical stimulation. *Sci Rep*, 4:4781.

115. Dvir T, Timko BP, Brigham MD, *et al*., 2011, Nanowired three-dimensional cardiac patches. *Nat Nanotechnol*, 6:720–725.

116. Kota AK, Cipriano BH, Duesterberg MK, *et al*., 2007, Electrical and rheological percolation in polystyrene/MWCNT nanocomposites. *Macromolecules*, 40:7400–7406.